Sensors & Diagnostics

PAPER

View Article Online
View Journal | View Issue

Cite this: *Sens. Diagn.*, 2023, **2**, 1207

A fluorescence "turn-on" probe for the respective ratiometric detection of hypochlorite and cysteine†

Zhizhen Wu,[a] Muzi Cai,[a] Wenjuan Lv,[a] Cancan Lu,[a] Bingyan Wu,[a] Cuiling Ren, *[a] Yalei Dong,*[b] Hongli Chen [a] and Xingguo Chen [a]

Received 28th February 2023,
Accepted 29th May 2023

DOI: 10.1039/d3sd00051f

rsc.li/sensors

As abnormal levels of hypochlorous acid (HClO) and cysteine (Cys) are associated with some diseases, it is of great importance to detect them accurately. In this work, new carbon dots (N-CDs) for respectively ratiometrically determining HClO and Cys *via* a "turn-on" mode were prepared. A good linear relationship was obtained between the F_{548}/F_{640} values and the concentration of HClO in the range of 90–800 μM, with a limit of detection (LOD) of 2.17 μM. By plotting the F_{640}/F_{548} values against the Cys concentration, a good linear relationship was obtained in the range of 170–900 μM, with a calculated LOD of 6.63 μM. Furthermore, the response mechanisms of the N-CDs towards HClO and Cys were studied systematically. Compared with reported fluorescent probes that can respectively or sequentially detect two types of small molecules, this "turn-on" luminescence nanosensor has low background interference, so it holds great potential for use in the diagnosis of HClO and Cys correlated diseases.

1. Introduction

Redox balance *in vivo* is closely associated with some diseases, such as cancer, neurodegenerative diseases, cardiovascular diseases, diabetes mellitus and so on. Cells possess an elaborate regulation system to maintain their redox balance and large or significant redox state changes can be buffered by redox-active molecules. These molecules undergo inter-reaction and inter-conversion to facilitate the dynamic balance of the intracellular redox state, among which three types of representative molecules should be mentioned, including reactive oxygen (H_2O_2, HClO, $O_2^{\bullet-}$, $^1O_2$, $^{\bullet}OH$), reactive nitrogen ($ONOO^-$, NO_2^-, HNO^-), and reactive sulfur (GSH, Cys, Hcy, H_2S, $RS^{\bullet}$) species.[1,2] As a normal byproduct of cellular metabolism, hypochlorous acid (HClO) is mainly involved in the regulation of cellular signaling transduction and immune response. It can be produced in immunological cells from hydrogen peroxide and chloride ions mediated by myeloperoxidase.[3–5] However, abnormal levels of endogenous HClO are associated with specific diseases, such as neuronal deformation, cardiovascular disease, arteriosclerosis, lung injury, and cancer.[6] Meanwhile, cysteine (Cys) plays crucial roles in many physiological and pathological processes as one of the sulfhydryl-containing amino acids.[7–9] Normal levels of Cys are essential for maintaining the synthesis of various proteins and act as a source of sulfide in human metabolism, while an excess or deficiency of Cys are associated with some diseases. Therefore, it is of great importance to detect HClO and Cys to accurately evaluate their role in physiological and pathological processes.

To date, electrochemical methods,[10,11] high-performance liquid chromatography,[12,13] surface-enhanced Raman spectroscopy[14] and fluorescence spectroscopy[15,16] are the common methods for detecting HClO or Cys. Among these methods, fluorescence spectroscopy has some advantages, such as high sensitivity, real-time analysis, high-throughput analysis, and readily available instruments. Recently, ratiometric fluorescent probes have attracted much attention because they can provide built-in correction and reduced background interference.[17–19] Furthermore, monitoring two related small molecules simultaneously can provide more information about cross-talk and interactions between these species. Recently, some ratiometric fluorescent sensors have been reported that can be used to detect two related molecules respectively or sequentially. For example, Ren *et al.* presented the first single-fluorescent probe Lyso-HA-HS that can detect HClO and H_2S within an organelle with multi-

[a] *State Key Laboratory of Applied Organic Chemistry, College of Chemistry and Chemical Engineering, Lanzhou University, Lanzhou 730000, P. R. China. E-mail: rencl@lzu.edu.cn; Fax: +86 931 8912582; Tel: +86 931 8912763*
[b] *National Institutes for Food and Drug Control/NMPA Key Laboratory for Researching and Evaluation of Cosmetics, Beijing 100050, China. E-mail: dongyalei@nifdc.org.cn*

† Electronic supplementary information (ESI) available. See DOI: https://doi.org/10.1039/d3sd00051f

response signals.[20] Wei *et al.* designed new carbon dots (RD-CDs) that can respond to ClO^- and AA rapidly *via* fluorescence and colorimetry, and can be used as a fluorescent probe for dynamically detecting ClO^- and AA in living cells.[21] Therefore, developing a ratiometric fluorescent nanosensor that can respectively detect HClO and Cys is important and meaningful.

Carbon dots (CDs) are highly appropriate fluorescent probes in biologically-relevant detection because of their good biocompatibility, ease of synthesis and unique optical properties.[22,23] However, CD sensors generally detect multiple analytes *via* a "turn-off–on" mode.[24,25] In comparison, detections based on "turn-on" luminescence are more desirable because they show better accuracy by reducing the influence of many quenching species.[26,27] Herein, dual emission carbon dots (N-CDs) were synthesized for separately detecting HClO and Cys by virtue of 'ratiometric' and 'turn-on' fluorescence responses. As shown in Scheme 1, the N-CDs show two fluorescence emission peaks at 548 and 640 nm. The fluorescence of the N-CDs at 548 nm can be enhanced just by HClO, while the fluorescence at 640 nm can only be enhanced by Cys. This new sensor not only combines the advantages of ratiometric fluorescence and a "turn-on" mode, but can also be used to ratiometrically detect HClO and Cys just using one sensor, which is favorable for providing more accurate information about cross-talk and interactions between these species. Furthermore, the intrinsic emission mechanism of the N-CDs was studied systematically.

2. Experimental section

Materials and reagents

N-Methylbenzene-1,2-diamine (OTD) was purchased from Aladdin. $NaClO{\cdot}5H_2O$, cysteine hydrochloride monohydrate, alanine, phenylalanine, threonine, arginine, methionine, leucine, serine, valine and isoleucine were purchased from Adamas. Histidine was purchased from Shanghai Zhongqin Chemical Reagent Co. GSH was purchased from Seymour Fisher Technology Co. *tert*-Butyl hydroperoxide (70%), 2,2′-azobis(2-methylpropionamidine) dihydrochloride, and sodium nitroprusside dihydrate were purchased from Energy. H_2O_2 (30%) was purchased from Tianjin Chemical Reagent Co. $Mg(NO_3)_2{\cdot}6H_2O$, calcium chloride and sodium citrate were purchased from Tianjin Institute of Light Fine Chemical Industry. Tetrabutylammonium tetrafluoroborate ($(Bu)_4NBF_4$) was purchased from Energy Chemical Technology Co. Sodium nitrite, $MnCl_4{\cdot}4H_2O$ and sodium bicarbonate were purchased from Cologne Chemical Reagent Factory, Chengdu, China. Sodium sulfate was purchased from Tianjin Damao Chemical Reagent Factory. All reagents were of analytical grade and used without any further purification, and ultrapure water was used throughout the experiments.

Instruments

UV-vis spectra were recorded on a 723PC UV-vis spectrophotometer. Transmission electron microscopy (TEM, Talos F200s) was used to characterize the morphology and size of the prepared CDs. Fourier-transform infrared (FT-IR) spectra were recorded on a Nicolet Nexus 670 spectrometer using the KBr pellet technique. The elemental composition of the N-CDs was determined using X-ray photoelectron spectrometry (XPS, Shimadzu, Japan). The fluorescence spectra were obtained using a scanning RF-5301 fluorescence spectrometer (Shimadzu, Japan). The highest occupied molecular orbital (HOMO) level of the material was measured by an ultraviolet photoelectron spectrometer (UPS) (Shimadzu, Japan). The quantum yield was measured using a steady-state/transient fluorescence spectrometer (FLS 920). A research-grade positive fluorescence microscope (Olympus BX53) was used to conduct the cell fluorescence imaging experiments.

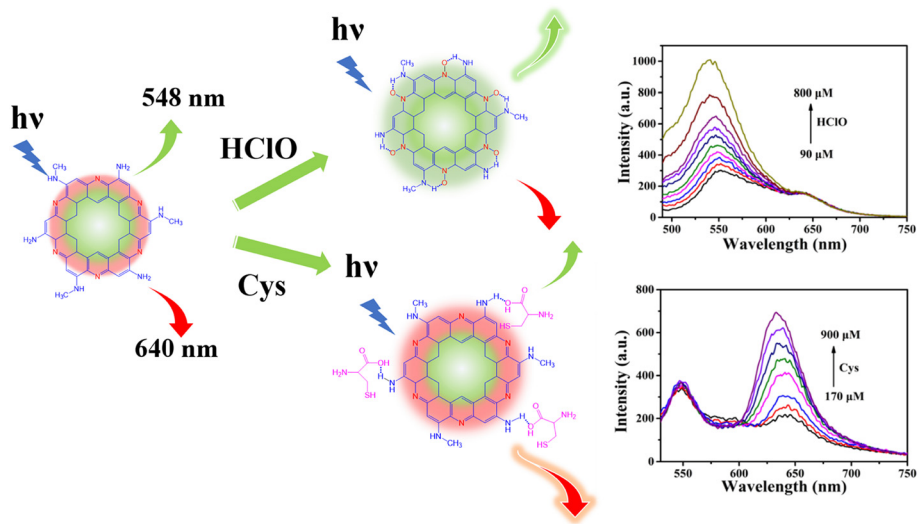

Scheme 1 Illustration of N-CDs as a "turn-on" and "ratiometric" fluorescence probe for HClO and Cys, respectively.

Preparation of N-CDs

0.3 g OTD was dissolved in 50 mL of ethanol, then the solution was transferred to a 100 mL Teflon-lined stainless steel autoclave. The sealed autoclave was heated at 160 °C for 6 h, before being allowed to naturally cool to room temperature. The products were centrifuged and the supernatant was collected and dialysed (molecular weight cut off of 500) for 24 h. The acquired solution was concentrated and dried.

Detection of HClO and Cys

Detection of HClO. 50 μL of N-CDs was added to a citric acid–sodium citrate (100 mM, pH = 5) buffer solution and then certain concentrations of HClO were added, the solutions were thoroughly mixed, and then were transferred to a spectrophotometer quartz cuvette. Finally, fluorescence spectra were recorded at an excitation wavelength of 460 nm.

Detection of Cys. 20 μL of the N-CDs was added to PBS buffer solution (10 mM, pH = 5), and then certain concentrations of Cys were added. The above solutions were thoroughly mixed and transferred to a spectrophotometer quartz cuvette, and fluorescence spectra were recorded at an excitation wavelength of 500 nm.

Selectivity tests

To assess the selectivity of the N-CDs towards HClO, the values of F_{548}/F_{640} (F_{548} and F_{640} are the fluorescence intensities of the N-CDs at 548 and 640 nm, respectively) after the addition of reactive oxygen species (ROS), reactive nitrogen species (RNS), amino acids and anions was tested. The selectivity of N-CDs to Cys was studied under the same conditions, instead using a value of F_{640}/F_{548}.

Detection of HClO and Cys in real samples

Serum provided by the general hospital of Lanzhou military region was used to test the feasibility of this method in complex biological samples. The authors state that all experiments were performed in compliance with the relevant laws and institutional guidelines. The serum was diluted 100-fold before analyzing, and the concentrations of HClO and Cys were analyzed using a standard addition method.

3. Results and discussion

3.1 Optimization of the synthesis conditions and detection wavelength

According to the experimental results, it can be seen that the fluorescence (FL) intensity of the N-CDs could be tuned according to the reaction time and temperature. In order to prepare N-CDs with high emission intensity, the two conditions were optimized. As shown in Fig. S1,† 160 °C and 6 h were chosen as the optimal reaction conditions.

During the experiment, we found that the fluorescence enhancement efficiency of the N-CDs by HClO and Cys could be tuned by changing the pH and excitation wavelength. The fluorescence enhancement efficiencies by HClO and Cys are all remarkable when detected under acidic conditions. The excitation wavelength was optimized at pH = 5 in order to attain higher fluorescence intensity enhancement. It can be seen from Fig. S2† that HClO and Cys have the highest fluorescence enhancement efficiency when the excitation wavelengths are 460 and 500 nm, respectively. Therefore, λ_{ex} = 460 nm and pH = 5 were selected as the best conditions for HClO detection. Meanwhile, λ_{ex} = 500 nm and pH = 5 were selected for Cys detection.

3.2 Characterization of the N-CDs

The TEM images presented in Fig. 1A reveal that the N-CDs are well dispersed, with an average particle size of approximately 4.12 nm, which was calculated based on 200 nanoparticles. The FT-IR spectra shown in Fig. 1B illustrate that the N-CDs possess N–H (3200 cm^{-1}) hydrophilic groups on their surface, which ensure their good water solubility.[28] The vibration of ═N–CH corresponds to 1385.31 cm^{-1}, and the characteristic peak at 1104–1165 cm^{-1} can be assigned to C–N flexural vibration.[29,30] Compared with that of OTD, the characteristic absorption band of the N-CDs at 2831–2881 cm^{-1} disappeared, and the characteristic absorption band at 1104–1165 cm^{-1} narrowed. This may be due to the imino group of OTD reacting with the adjacent amino group during the synthesis of the N-CDs, which also proves their successful formation.

XPS was used to further investigate the composition and surface groups of the N-CDs. The survey XPS spectra presented in Fig. 1C shows three typical peaks at C1s (285 eV), N1s (400 eV) and O1s (532 eV). This result illustrates that the N-CDs are composed of C, N and O. In the high-resolution spectra (Fig. S3†), the C1s band can be deconvoluted into three peaks, corresponding to sp^2 carbon (C═C, 284.8 eV), sp^3 carbon (C–O/C–N, 285.7 eV), and carbonyl carbon (C═O, 286.9 eV).[31] Two types of N, pyridinic N (398.9 eV) and amino N (400.6 eV), can be observed from the N1s spectrum shown in Fig. S3B.†[32] In addition, two peaks located at 531.7 and 532.9 eV can be observed in the O1s spectrum (Fig. S3C†), which can be assigned to the vibration of C═O and C–O.[33] The XPS results further confirm the formation of N-CDs and that there are plenty of functional groups on their surface, which is consistent with the FT-IR spectroscopy results.

3.3 Stability of the N-CDs

The stability of the sensor is crucial for its detection application. In this work, the stabilities of the N-CDs under different conditions were tested. As shown in Fig. S4A,† the FL intensity of the N-CDs was very stable, even when the concentration of NaCl was as high as 100 mM in the solution, showing excellent salt tolerance. Moreover, their FL intensity almost unchanged in the temperature range of 0–50 °C (Fig. S4B†), implying they also exhibit excellent temperature stability. Moreover, it can be seen from Fig. S4C† that the

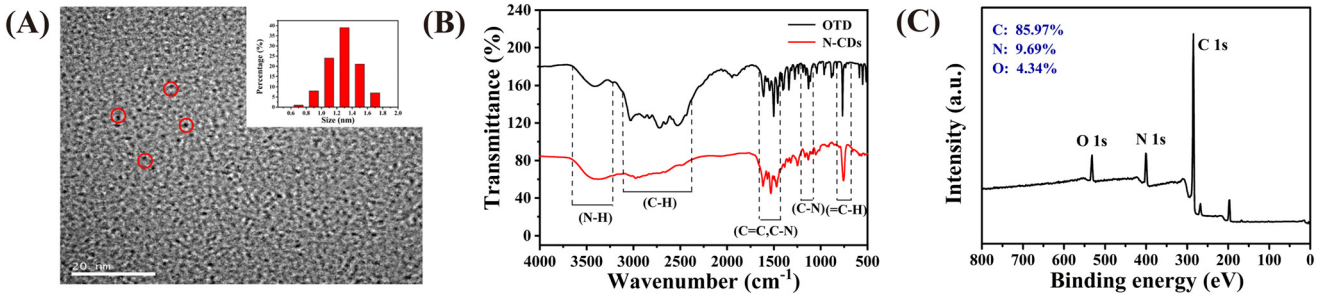

Fig. 1 (A) TEM image of the N-CDs (inset: size distribution of the N-CDs); (B) FT-IR spectra of the N-CDs and OTD; (C) XPS survey spectrum of the N-CDs.

fluorescent signal of N-CDs remains relatively stable after irradiation for 60 min, indicating their excellent anti-photobleaching capability.

3.4 Detection performance of the N-CDs towards HClO and Cys

Fig. 2A demonstrates that the N-CDs exhibit two photoluminescence peaks at 548 nm and 640 nm when excited at 460 nm. The photoluminescence signal of the N-CDs at 548 nm gradually enhances with an increase in the concentration of HClO (C_{HClO}), while the intensity at 640 nm remains unchanged. As plotted in Fig. 2B, a good linear relationship between F_{548}/F_{640} and C_{HClO} can be observed. The linear regression equation is $y = 0.0018x + 1.637$, with a correlation coefficient of 0.9935. Moreover, the limit of detection (LOD) was calculated to be 2.17 μM based on $3\sigma/k$ (σ is the standard deviation of the blank signal, and k is the slope of the calibration curve). The selectivity of the N-CDs as a ratiometric nanoprobe towards HClO was evaluated by monitoring the value of F_{548}/F_{640} *vs.* HClO and other ROS, RNS, amino acids and anions. As shown in Fig. 2C, the F_{548}/F_{640} values are only affected by HClO. Fig. 2D shows that the coexistence of these interferents has no influence on the response of the N-CDs towards HClO. These results prove that the N-CDs can be used to detect HClO selectively.

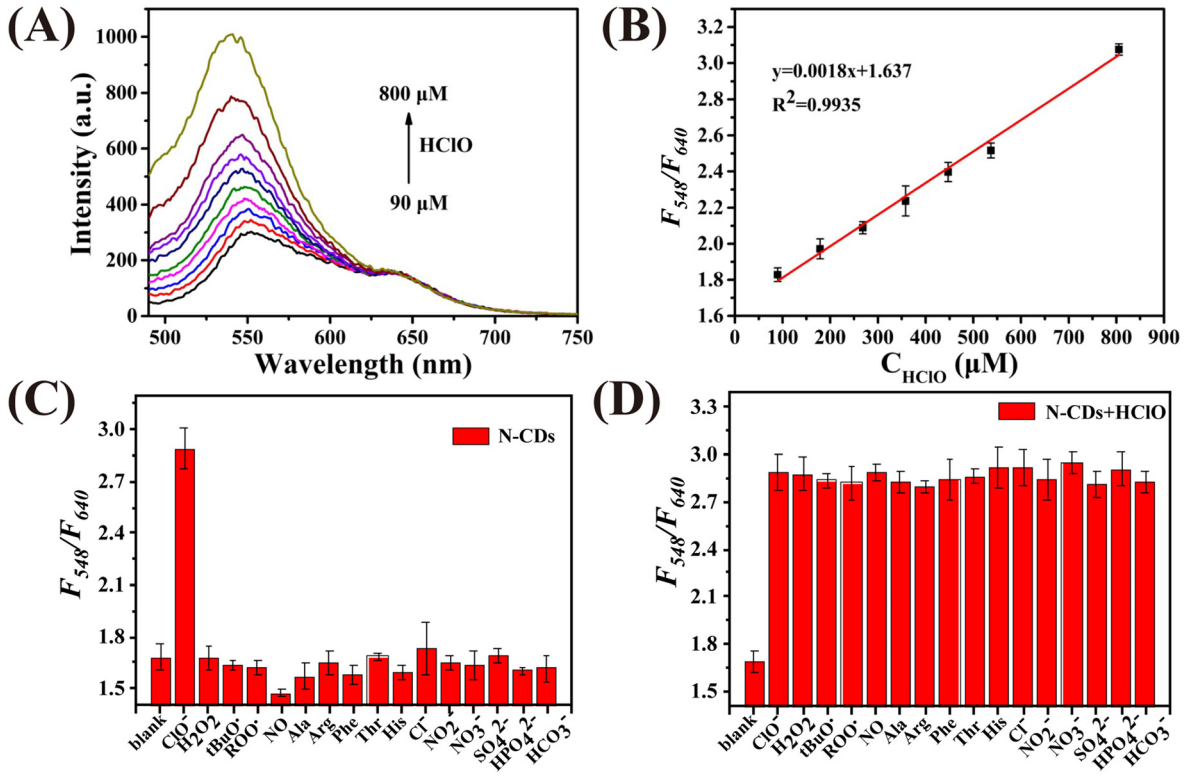

Fig. 2 (A) Fluorescence emission spectra of the N-CDs upon the addition of various concentrations of HClO in the range of 90–800 μM; (B) relationship between F_{548}/F_{640} and C_{HClO}; (C) fluorescence response of the N-CDs towards HClO and other ROS, RNS, amino acids and anions (H_2O_2, *t*BuO, ROO, NO, Ala, Arg, Phe, Thr, His, Cl^-, NO_2^-, NO_3^-, SO_4^{2-}, HPO_4^{2-}, HCO_3^-); (D) fluorescence response of the N-CDs towards HClO in the presence of other ROS, RNS, amino acids and anions (H_2O_2, *t*BuO, ROO, NO, Ala, Arg, Phe, Thr, His, Cl^-, NO_2^-, NO_3^-, SO_4^{2-}, HPO_4^{2-}, HCO_3^-).

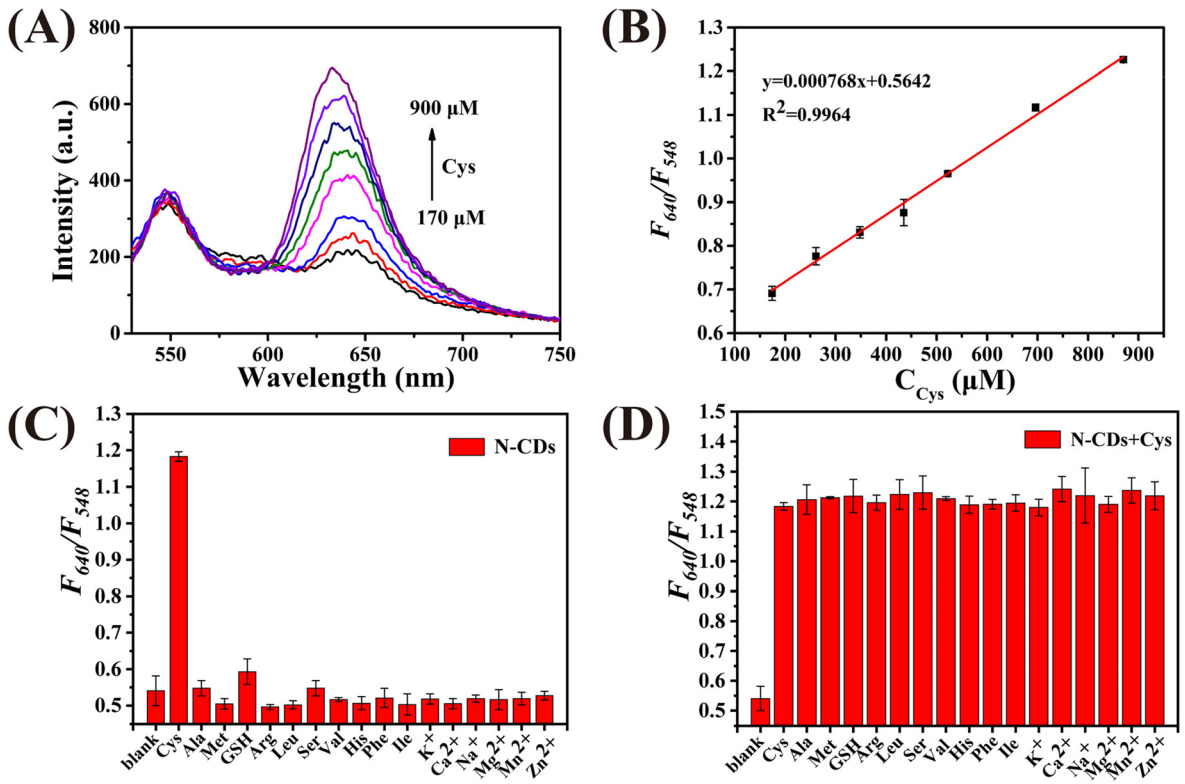

Fig. 3 (A) FL emission spectra of the N-CDs with the addition of 0–800 μM Cys; (B) relationship between F_{640}/F_{548} and the concentrations of Cys; (C) fluorescence intensity of the N-CDs with the addition of reducing substances, amino acids, and cations (Cys, GSH, Ala, Met, Arg, Leu, Ser, Val, His, Phe, Ile, K^+, Ca^{2+}, Na^+, Mg^{2+}, Mn^{2+}, Zn^{2+}); (D) fluorescence intensity of the N-CDs with the addition of Cys in the presence of other reducing substances, amino acids, and cations (Cys, GSH, Ala, Met, Arg, Leu, Ser, Val, His, Phe, Ile, K^+, Ca^{2+}, Na^+, Mg^{2+}, Mn^{2+}, Zn^{2+}).

Then, the detection performance of the N-CDs as a ratiometric "turn-on" nanoprobe towards Cys was investigated. As shown in Fig. 3A, with an increase in the concentration of Cys (C_{Cys}), the fluorescence intensity of the N-CDs at 640 nm enhanced, whereas that at 548 nm was unchanged. Plotting the F_{640}/F_{548} values against C_{Cys}, a good linear relationship (R^2 = 0.9964) can be obtained in the range of 170–900 μM (Fig. 3B). The LOD was calculated to be 6.63 μM. Selectivity is considered to be one of the greatest challenges for Cys detection in biological media. In this work, reducing substances, amino acids, and cations, which commonly exist in real samples, were used to investigate the selectivity of N-CDs towards Cys. As demonstrated in Fig. 3C and D, the F_{548}/F_{640} value of the N-CDs shows no obvious response to these interferents, except to Cys, indicating that the N-CDs exhibit excellent sensitivity and specificity for Cys detection. Furthermore, it is important to point out that the entire detection process can be completed in a few minutes, which means that this 'turn-on' mode ratiometric nanosensor can be used to detect HClO and Cys specifically, sensitively and efficiently.

3.5 Possible optical response mechanism of the N-CDs towards HClO and Cys

The above-mentioned results indicate that the fluorescence emission of the N-CDs at 548 nm is responsive to HClO, but what is the reason for this? Fig. 4A illustrates that the absorption of the N-CDs is strongly dependent on the solvent polarity, which means that the fluorescence of the N-CDs at 548 nm may be derived from the molecular state.[34] The molecular state can be regarded as a structural unit composed of a single or multiple fluorophores. Furthermore, after the addition of HClO, the fluorescence emission of N-CDs at 548 nm blue shifts to 537 nm, and its intensity increases (Fig. 2A). Moreover, the absorption peak also blue shifts from 554 nm to 520 nm (Fig. 4B). These results are in line with the characteristics of intramolecular charge transfer (ICT),[35] with a preliminary inference that HClO can prevent the charge transfer process within the fluorophore.

In order to investigate this hypothesis, the highest occupied molecular orbital (HOMO) energy levels of the N-CDs were estimated according to the empirical formula:[36]

$$E_{HOMO} = E_{SECO} - 21.22 \text{ eV}$$

where the E_{SECO} is the initial energy difference between the two ends of the UPS spectrum of the N-CDs (Fig. 4C), with the corresponding E_{HOMO} calculated to be −8.33 eV. The lowest unoccupied molecular orbital (LUMO) levels could be calculated from the E_{HOMO} using the optical energy gap (E_g, resulting from the absorption edge in the absorption spectrum) as follows:[28]

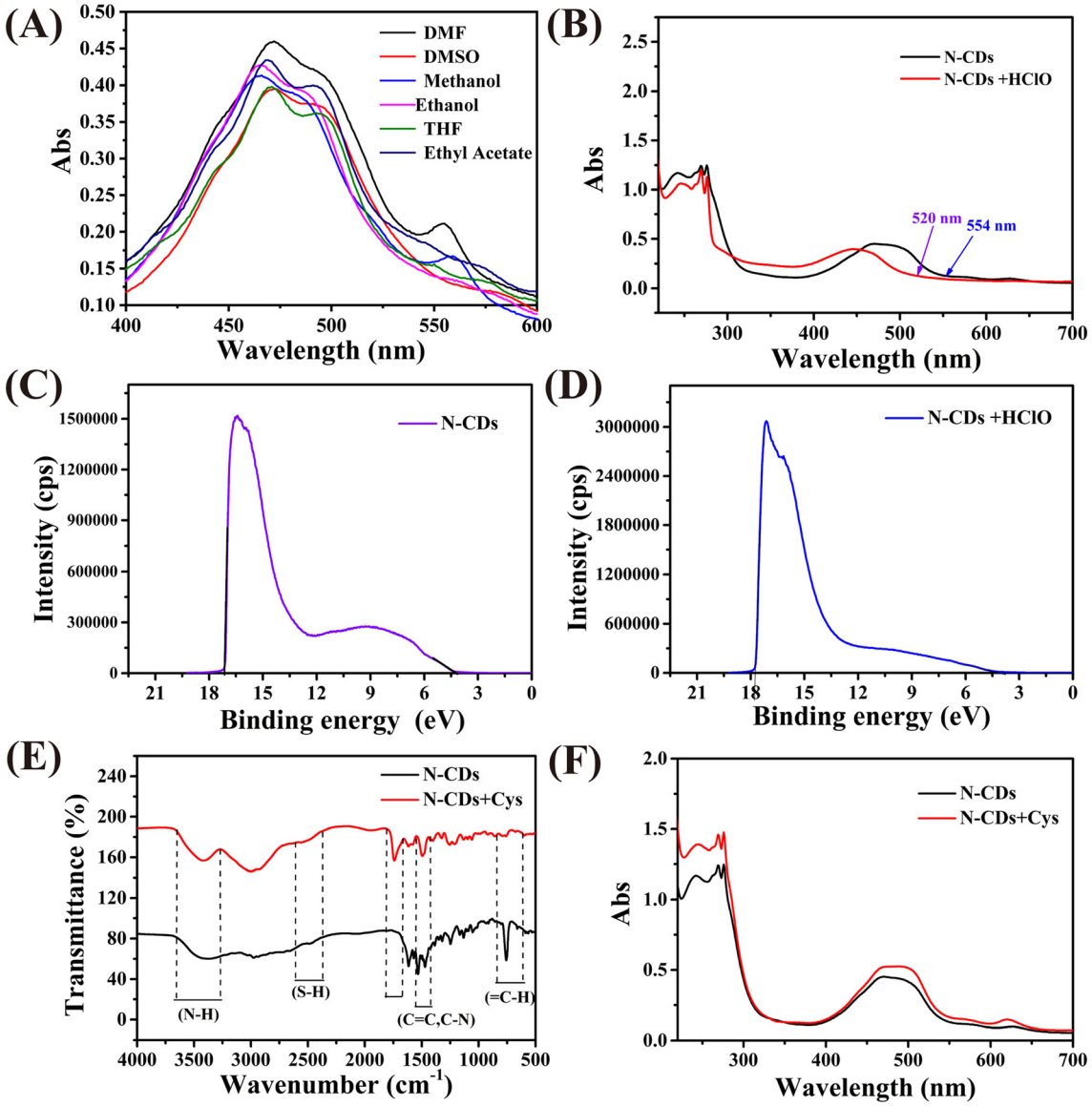

Fig. 4 UV-vis absorption spectra of (A) N-CDs in different polar solvents; (B) N-CDs before and after the addition of HClO; UPS spectrum of (C) N-CDs; (D) N-CDs + HClO; (E) FT-IR spectra and (F) UV-vis absorption spectra of the N-CDs before and after the addition of Cys.

$$E_{LUMO} = E_{HOMO} + E_g$$

$$E_g = h\nu = hc/\lambda$$

where h is Planck's constant ($4.13566743 \times 10^{-15}$ eV s), ν is the frequency, c is the speed of light (3.0×10^8 m s^{-1}), and λ is the wavelength of the absorption edge in the absorption spectrum. For the N-CDs in this work, λ is 554 nm (Fig. 4B), so E_g is estimated to be 2.24 eV. Thus, the E_{LUMO} is −6.09 eV. Similarly, the HOMO and LUMO energy levels of the N-CDs after the addition of HClO were also estimated, where E_{SECO} is 13.33 eV (Fig. 4D), E_{HOMO} is −7.89 eV, λ is 520 nm (Fig. 4B), and E_g is 2.39 eV, so E_{LUMO} was evaluated to be −5.5 eV. The calculated results show that the energy level of the N-CDs increases after the addition of HClO (Fig. S5†), which is consistent with the reported ICT mechanism.[37]

In order to further investigate the structure of the fluorophore centers, the E_g values of 16 potential structures were calculated by means of density functional theory. The results are shown in Fig. S6,† where the E_g value of the molecular structure labeled 5–3 (2.27 eV) is the closest to the experimental value (2.24 eV), so the 5–3 molecule may be the fluorophore center of the N-CDs. In addition, cyclic voltammetry shows that the N-CDs were oxidized after the addition of HClO (Fig. S7†), which reduces the power supply capacity of the fluorescence center and impedes the ICT process in the probe. The energy level eventually rises, which is the main cause of the blue shift in the fluorescence and UV-vis spectra and the enhancement in the photoluminescence intensity. Based on the above experimental results, it can be concluded that the

enhancement effect of HClO on N-CDs conforms to the ICT mechanism.

FT-IR spectroscopy was employed to investigate the fluorescence response mechanism of the N-CDs to Cys. The FT-IR spectrum of the N-CDs before and after the addition of Cys shows no significant changes (Fig. 4C), which means that no chemical reaction occurred between the N-CDs and Cys.[38] The fluorescence behavior of the N-CDs correlates to inner filter, photoelectron transfer, fluorescence resonance energy transfer, and surface complexation effects. According to Fig. 3A and S8,† we can see that there is no overlap between the absorbance of Lys and the PL emission of the N-CDs, so the fluorescence resonance energy transfer and inner filter effect could be excluded. After the addition of Cys, the absorption spectrum shows no new peaks but the absorbance intensity was enhanced (Fig. 4F), implying the absence of surface complexation effects. Meanwhile, the emission wavelength gradually blue-shifts and the fluorescence intensity significantly enhances as the concentration of Cys increases, which might be due to Cys binding to the N-CDs (Fig. 3A).[39] The fluorescence lifetime is closely associated with the surface states of the N-CDs, so in order to disclose the sensing mechanism, the fluorescence lifetimes of the N-CDs before and after the addition of Cys were recorded separately. As shown in Fig. S9,† the lifetime of the N-CDs increased after the addition of Cys. Based on previous reports, the intramolecular hydrogen interaction and the proximity of hydrogen bonds can change the fluorescence intensity and lifetime, so the above mentioned results reveal that the response of the N-CDs towards Cys stems from Cys biding to the N-CDs.[40,41]

3.6 Detection of HClO and Cys in biological samples

To investigate the potential of the N-CDs in practical applications, they were used to detect HClO in human serum, with the results listed in Table 1. The recoveries of HClO in the serum samples are in the range of 99.20–103.75%, and their relative standard deviation (RSD) values (n = 5) are all <2.59%. This indicates that our proposed method exhibits good accuracy and high precision. Cys in serum samples was also determined using a standard addition method (Table 2). The recoveries of Cys in the serum samples are in the range of 99.60–102.70%, and their RSD values (n = 5) are all <2.12%. Therefore, the N-CDs can be used as a ratiometric fluorescent nanoprobe for the detection of HClO and Cys in complex biological samples.

Table 1 Detection results of HClO in serum samples by N-CDs

Sample	Added amount (μM)	Found amount (μM)	Average recovery (%, n = 3)	RSD (%, n = 3)
Serum	0.00	0.00	—	—
	180	186.75	103.75	2.59
	360	357.12	99.20	0.85
	720	720.14	100.01	0.31

Table 2 Detection results of Cys in serum samples by N-CDs

Sample	Added amount (μM)	Found amount (μM)	Average recovery (%, n = 3)	RSD (%, n = 3)
Serum	0.00	0.00	—	—
	180	184.86	102.70	2.12
	360	363.65	101.01	1.46
	720	717.12	99.60	1.85

4. Conclusion

In summary, dual emission N-CDs were synthesized *via* a facile hydrothermal method. The prepared N-CDs show good stability, and its fluorescent intensity at 548 and 640 nm can be enhanced only by HClO and Cys, respectively. These results prove that the N-CDs can be used as a fluorescence "turn-on" probe for the respective ratiometric detection of HClO and Cys. The enhancement effect of HClO on the N-CDs conforms to the ICT mechanism, and Cys bonding to the N-CDs is responsible for the fluorescence enhancement. The excellent detection performance makes the N-CDs a good sensor for detecting diseases associated with HClO and Cys.

Ethical statement

All animal procedures were performed in accordance with the Guidelines for Care and Use of Laboratory Animals of "Lanzhou" University and approved by the Animal Ethics Committee of "jcyxy20220207".

Conflicts of interest

The authors declare no competing financial interest.

Acknowledgements

This work was supported by the National Natural Science Foundation of China (No. 21874061) and the Science and Technology program of Gansu Province (No. 22JR5RA476).

References

1 X. Jiao, Y. Li, J. Niu, X. Xie, X. Wang and B. Tang, *Anal. Chem.*, 2018, **90**, 533–555.
2 V. Staikopoulos, X. Zhang, B. P. Pullen, P. Reineck, A. K. Vidanapathirana, S. M. Lee, J. Liu, C. Bursill, M. R. Hutchinson and A. D. Abell, *Sens. Diagn.*, 2022, **1**, 280–293.
3 T. Finkel and N. J. Holbrook, *Nature*, 2000, **408**, 239–247.
4 D. I. Pattison and M. J. Davies, *Chem. Res. Toxicol.*, 2001, **14**, 1453–1464.
5 H. Tan, X. Wu, Y. Weng, Y. Lu and Z. Z. Huang, *Anal. Chem.*, 2020, **92**, 3447–3454.
6 J. D. Lambeth, *Free Radical Biol. Med.*, 2007, **43**, 332–347.
7 W. F. Niu, L. Guo, Y. H. Li, S. M. Shuang, C. Dong and M. S. Wong, *Anal. Chem.*, 2016, **88**, 1908–1914.
8 Z. J. Tang, Z. H. Lin, G. K. Li and Y. L. Hu, *Anal. Chem.*, 2017, **89**, 4238–4245.

9 E. Weerapana, C. Wang, G. M. Simon, F. Richter, S. Khare, M. B. D. Dillon, D. A. Bachovchin, K. Mowen, D. Baker and B. F. Cravatt, *Nature*, 2010, **468**, 790–795.
10 S. Kumaravel, T. S. T. Balamurugan, S. H. Jia, H. Y. Lin and S. T. Huang, *Anal. Chim. Acta*, 2020, **1106**, 168–175.
11 A. M. Mahmoud, S. A. Alkahtani and M. M. El-Wekil, *Anal. Bioanal. Chem.*, 2022, **414**, 2343–2353.
12 L. Nejdl, J. Sochor, O. Zitka, N. Cernei, B. Ruttkay-Nedecky, P. Kopel, P. Babula, V. Adam, J. Hubalek and R. Kizek, *Chromatographia*, 2013, **76**, 363–373.
13 Q. Y. Xiao, H. L. Gao, Q. P. Yuan, C. Lu and J. M. Lin, *J. Chromatogr. A*, 2013, **1274**, 145–150.
14 Z. S. Jie, J. Liu, Y. Ying and H. F. Yang, *Spectrochim. Acta, Part A*, 2023, **287**, 122048.
15 H. Dong, Y. L. Zhou, L. Zhao, Y. Q. Hao, Y. T. Zhang, B. X. Ye and M. T. Xu, *Anal. Chem.*, 2020, **92**, 15079–15086.
16 B. Zhou, B. Wang, M. Bai, M. Dong and X. Tang, *Spectrochim. Acta, Part A*, 2023, **294**, 122523.
17 X. N. Bu, Y. X. Fu, X. W. Jiang, H. Jin and R. J. Gui, *Microchim. Acta*, 2020, **187**, 154.
18 R. J. Gui, X. N. Bu, W. J. He and H. Jin, *New J. Chem.*, 2018, **42**, 16217–16225.
19 X. W. Jiang, H. Jin, Y. J. Sun and R. J. Gui, *Microchim. Acta*, 2019, **186**, 580.
20 M. G. Ren, Z. H. Li, B. B. Deng, L. Wang and W. Y. Lin, *Anal. Chem.*, 2019, **91**, 2932–2938.
21 Z. N. Wei, H. Q. Li, S. B. Liu, W. Wang, H. L. Chen, L. H. Xiao, C. L. Ren and X. G. Chen, *Anal. Chem.*, 2019, **91**, 15477–15483.
22 V. Sharma, P. Tiwari and S. M. Mobin, *J. Mater. Chem. A*, 2017, **5**, 8904–8924.
23 Swathilakshmi and S. Anandhan, *Sens. Diagn.*, 2022, **1**, 902–931.
24 G. L. Chen, H. Feng, X. G. Jiang, J. Xu, S. F. Pan and Z. S. Qian, *Anal. Chem.*, 2018, **90**, 1643–1651.
25 X. F. Yang, M. T. Zhang, Y. L. Zhang, N. Wang, W. Bian and M. M. F. Choi, *Anal. Methods*, 2019, **11**, 5803–5809.
26 Y. Huang, L. Sun and L. M. Mirica, *Sens. Diagn.*, 2022, **1**, 709–713.
27 W. Li, Z. Ma, L. Du and M. Li, *Anal. Chem.*, 2023, **95**, 2848–2856.
28 H. J. Zhang, Y. L. Chen, M. J. Liang, L. F. Xu, S. D. Qi, H. L. Chen and X. G. Chen, *Anal. Chem.*, 2014, **86**, 9846–9852.
29 B. Ju, Y. Wang, Y. M. Zhang, T. Zhang, Z. H. Lu, M. J. Li and S. X. A. Zhang, *ACS Appl. Mater. Interfaces*, 2018, **10**, 13040–13047.
30 B. Ju, T. Zhang, S. Li, J. Liu, W. R. Zhang, M. J. Li and S. X. A. Zhang, *New J. Chem.*, 2019, **43**, 168–174.
31 L. Wang, M. Li, W. T. Li, Y. Han, Y. J. Liu, Z. Li, B. H. Zhang and D. Y. Pan, *ACS Sustainable Chem. Eng.*, 2018, **6**, 12668–12674.
32 K. K. Liu, S. Y. Song, L. Z. Sui, S. X. Wu, P. T. Jing, R. Q. Wang, Q. Y. Li, G. R. Wu, Z. Z. Zhang, K. J. Yuan and C. X. Shan, *Adv. Sci.*, 2019, **6**, 10.
33 Y. Q. Zhang, J. H. Xiao, P. Zhuo, H. Yin, Y. Fan, X. Y. Liu and Z. Q. Chen, *ACS Appl. Mater. Interfaces*, 2019, **11**, 46054–46061.
34 Y. B. Song, S. J. Zhu, S. Y. Xiang, X. H. Zhao, J. H. Zhang, H. Zhang, Y. Fu and B. Yang, *Nanoscale*, 2014, **6**, 4676–4682.
35 N. Bhuvanesh, S. Suresh, P. R. Kumar, E. M. Mothi, K. Kannan, V. R. Kannan and R. Nandhakumar, *J. Photochem. Photobiol., A*, 2018, **360**, 6–12.
36 L. Y. Zheng, T. Zhu, W. Z. Xu, L. Liu, J. Zheng, X. Gong and F. Wudl, *J. Mater. Chem. A*, 2018, **6**, 3634–3641.
37 X. H. Cheng, R. L. Tang, H. Z. Jia, J. Feng, J. G. Qin and Z. Li, *ACS Appl. Mater. Interfaces*, 2012, **4**, 4387–4392.
38 L. Yu, H. X. Chen, J. Yue, X. F. Chen, M. T. Sun, H. Tan, A. M. Asiri, K. A. Alamry, X. K. Wang and S. H. Wang, *Anal. Chem.*, 2019, **91**, 5913–5921.
39 M. Wang, C. H. Li, M. L. Zhou, Z. N. Xia and Y. K. Huang, *Green Chem.*, 2022, **24**, 6696–6706.
40 Y. Su, K. Y. Li and X. K. Yu, *J. Phys. Chem. B*, 2019, **123**, 884–890.
41 C. Wang, Y. He, Y. Xu, L. Sui, T. Jiang, G. Ran and Q. Song, *J. Mater. Chem. A*, 2022, **10**, 2085–2095.